

## Modeling variable-density flow in saturated-unsaturated porous media: An advanced numerical model

Anis Younes<sup>a</sup>, Behshad Koohbor<sup>a,b</sup>, Benjamin Belfort<sup>a</sup>, Philippe Ackerer<sup>a</sup>, Joanna Doummar<sup>c</sup>, Marwan Fahs<sup>a,\*</sup>

<sup>a</sup> Université de Strasbourg, CNRS, ENGEEs, Institut Terre et Environnement de Strasbourg, UMR 7063, 5 rue René Descartes, Strasbourg F-67084, France

<sup>b</sup> BRGM (French Geological Survey), Orléans, France

<sup>c</sup> Department of Geology, American University of Beirut, Beirut, Lebanon

### ARTICLE INFO

#### Keywords:

Unsaturated flow  
Variable-density flow  
Mixed finite element method  
Discontinuous finite element method  
Multi-point flux approximation  
Method of lines  
Field simulation

### ABSTRACT

Modeling variable-density flow in unconfined aquifers is a challenging task because of the nonlinear coupling between variably saturated flow and contaminant transport. This results in a highly nonlinear system since the strongly nonlinear Richards flow equation is, in addition, coupled to the advection-dispersion transport equation by viscosity and density variation. The solution of such a nonlinear system is often subject to convergence issues and can be very expansive in terms of computational time, especially for large-scale problems. Conventional numerical algorithms based on the sequential approach and the classical finite difference or finite element methods with the first-order backward Euler time integration scheme are generally inefficient and/or do not provide satisfactory results. In this work, we develop a new efficient and accurate 2D numerical model for the transport of dense contaminants in unsaturated porous media that allows for the simulation of large-scale problems. This research describes a new model that combines advanced spatial discretization methods (mixed hybrid finite element method, discontinuous Galerkin finite element method, and multipoint flux approximation method) with higher-order time integration techniques via the method of lines (MOL). The latter allows one to adapt the time step's size and the order of the time integration to improve the computational efficiency while maintaining accuracy. The robustness and accuracy of the new model are shown by comparison against a widely used commercial code based on the standard finite element method. The applicability of the developed model to a large-scale problem is then investigated by simulating saltwater intrusion under a climate change projection and long-term pumping regimes for the Akkar coastal aquifer in Lebanon using a simplified 2D conceptual model.

### 1. Introduction

Many saturated-unsaturated aquifer systems are subject to the pollution of soils and groundwater resources by dense contaminants such as leachates derived from waste disposal sites, agricultural activity, or sanitary landfills. Contamination by saltwater is a major environmental issue that occurs, for instance, with the leakage of brine beneath the salt lakes, flooding of coastal areas by seawater, saltwater intrusion in coastal aquifers due to over-pumping, tidal effects or sea-level rise. For such situations, fluid flow and solute transport equations are coupled by the fluid density.

Several studies have focused on variable-density flow in saturated porous media (Diersch and Kolditz, 2002; Simmons, 2005; Graf et al., 2010; Werner et al., 2013) since the effect of density variations on the

flow behavior in the saturated zone is much more significant than in the unsaturated zone. Indeed, in the unsaturated zone, the density variation in the liquid phase is much less important than the density variation between the liquid and the air phase (about three orders of magnitude). Simmons et al. (2002) investigated the migration of a dense contaminant plume through the unsaturated zone using laboratory experiments. They showed that the unsaturated zone and position of the water table must be considered in contamination studies in order to predict the migration pathways, rates and the ultimate fate of dense contaminant plumes (Simmons et al., 2002). Oostrom et al. (1992) and Dane et al. (1994) investigated saturated variable-density flow with a narrow unsaturated zone in their physical models. They showed that the development of plume instabilities depends on the density difference between the plume and groundwater, the horizontal Darcy velocity, the contaminant

\* Corresponding author.

E-mail address: [fahs@unistra.fr](mailto:fahs@unistra.fr) (M. Fahs).

<https://doi.org/10.1016/j.advwatres.2021.104077>

Received 24 February 2021; Received in revised form 7 November 2021; Accepted 9 November 2021

Available online 14 November 2021

0309-1708/© 2021 Elsevier Ltd. All rights reserved.

leakage rates, the source dimensions, the hydrodynamic dispersion and the permeability of the porous media. Ouyang and Zheng (1999) numerically showed that density-driven transport is significant for dissolved chemicals through unsaturated sandy soils. Using numerical simulations, Boufadel et al. (1999) showed that concentration-dependent viscosity effects below dry salt lakes are significant under fully saturated conditions, but have minor effects under unsaturated flow conditions.

Considering both saturated and unsaturated zones for coupled flow and transport processes can improve the representativeness of simulations when investigating evaporation and salt accumulation effects on riparian freshwater lenses (America et al., 2020) or when investigating the effect of water table salinization (Werner and Lockington, 2004; Werner and Lockington, 2006; Ibrahim et al., 2014; Badaruddin et al., 2015) or the effect of the slope of the seaward boundary on saltwater intrusion (Qu et al., 2014; Zhou et al., 2014; Ataie-Ashtiani et al., 2001).

Including the unsaturated zone when modeling variable-density flow problems requires the solution of a coupled flow-transport nonlinear system. In such a system, the flow is ruled by the Richards' equation (RE), which uses nonlinear constitutive relationships between hydraulic conductivity, water content, and pressure head (Farthing and Ogden, 2017; Szymkiewicz, 2013). Because of these nonlinearities, providing an accurate solution of RE is challenging due to convergence issues and high time consumption, particularly in the presence of sharp wetting fronts, as when simulating infiltration into initially dry soils (Zha et al., 2017). These difficulties are increased in the case of a dense contaminant because of additional nonlinearities induced by density variations which require coupling between the RE and the advection-dispersion transport equation.

Because of nonlinearities and the absence of analytical solutions, numerical models are valuable tools for solving these complex problems and for understanding and predicting the propagation of contaminations in the aquifers. However, most of the existing numerical models do not provide satisfactory results when applied to unsaturated variable-density flow problems, essentially because:

- Classical spatial discretization methods such as finite element (FE) or finite difference (FD) methods may not provide an accurate velocity field, especially in the case of highly heterogeneous and/or anisotropic domains (Durlafsky, 1994; Schneider et al., 2018).
- When applied to the transport equation, the classical methods provide results with significant unphysical oscillations for advection-dominated transport. If combined with first-order upstream techniques, they suffer from excessive numerical dispersion (Konz et al., 2009).
- Temporal discretization is often based on the first-order backward Euler scheme, which does not allow large time steps and, as a consequence, induces excessive computational time.
- Coupling between flow and transport equations is usually performed via a sequential approach with an empirical time-stepping technique without any control over the temporal truncation error, which may lead to inaccurate results (Younes and Ackerer, 2010).

To overcome these difficulties, in this work, we combine advanced spatial and temporal approximation methods. The flow equation is solved using the mixed hybrid finite element (MHFE) method (Chavent and Roberts, 1991). This method simultaneously approximates both pressure and fluxes with the same order of convergence. The MHFE method is (i) locally conservative, (ii) well adapted for general unstructured meshes, and (iii) can easily handle full permeability tensors. The unknowns with the hybrid formulation are the traces of the pressure at edges/faces (Younes et al., 2010). The lumped form of the MHFE method proposed in (Younes et al., 2006) is employed in this work to avoid spurious oscillations encountered with transient simulations in the case of sharp wetting fronts (Belfort et al., 2009).

For the transport equation, the discontinuous Galerkin (DG) method

is used to discretize the advection equation and combined with the multi-point flux approximation (MPFA) method for the discretization of the dispersion equation (Younes and Ackerer, 2008). The DG method is strictly conservative at the element level. It yields accurate results for problems involving sharp fronts (Siegel et al., 1997). DG is used with an implicit time discretization that avoids (i) time-step limitation caused by the Courant–Friedrichs–Lewy (CFL) condition of explicit schemes and (ii) the use of a slope-limiting procedure to ensure the stability of the results (Younes and Ackerer, 2008). A discontinuous linear approximation is used for the concentration at each element of the mesh. Often, the DG degrees of freedom (DOFs) correspond to the discontinuous concentration at the nodes inside each element (see, for instance, (Ackerer et al., 1999; Hoteit and Firoozabadi, 2005)). The DOFs used here are the mean concentration and the horizontal and vertical components of the concentration gradient at each element (Younes and Ackerer, 2008). This choice allows one to imitate the upwind finite volume (FV) method when only the first equation corresponding to the mean concentration value is kept. Further, this choice of DOFs allows one to combine the DG method with MPFA for the approximation of dispersion without any operator splitting (Younes and Ackerer, 2008). The classical methods, like FD or FV, based on two-point flux approximation (TPFA) to compute the flux between two adjacent elements, may not converge unless the grid is K-orthogonal (Aavatsmark et al., 1998). The MPFA method calculates the flux at an element boundary using multiple surrounding elements; therefore, it is well adapted for general grids and full dispersion tensors (Younes and Fontaine, 2008).

The spatial discretization (MHFE\_DG\_MPFA) based upon the combination of MHFE, DG, and MPFA methods was shown to be robust and accurate for modeling variable-density flow in saturated porous media (Ackerer and Younes, 2008) and is extended in this work for unsaturated flow.

Higher-order time integration methods are used via the method of lines (MOL) to allow large time steps and improve the efficiency of the model. The flow and transport equations are solved simultaneously in a single step, which avoids slow convergence encountered with the sequential approach. The MOL allows one to adapt the time step's length and the order of the temporal discretization (up to 5 using the Backward Difference Formulas) in order to reduce the computational time while maintaining accuracy. The MOL is effective for the solution of the RE in the unsaturated zone (Fahs et al., 2009) as well as for variable-density flow in saturated porous media (Younes et al., 2009). In this work, the MOL is used for the first time for dense contaminant transport in unsaturated porous media. Variable-order and variable-step size time integration are performed using the DASPK (Van Keken et al., 1995) time solver.

## 2. Governing equations

Dense contaminant transport in unsaturated porous media is governed by the Darcy-Buckingham's law, the mass conservation of the fluid and the advection-dispersion transport equation. Assuming the Boussinesq approximation is valid, the flow in the unsaturated zone can be written in terms of equivalent freshwater head, as follows:

$$\frac{\partial \theta}{\partial t} = \left( c(h) + S_s \frac{\theta(h)}{\theta_s} \right) \frac{\partial H}{\partial t} = -\nabla \cdot \mathbf{q} + q_s \quad (1)$$

$$\mathbf{q} = -k_r \mathbf{K} \left( \nabla H + \frac{\rho - \rho_0}{\rho_0} \nabla z \right) \quad (2)$$

where  $c(h) = \partial \theta / \partial h$  is the specific moisture capacity [ $L^{-1}$ ],  $S_s$  the specific mass storativity related to head changes [ $L^{-1}$ ],  $\theta$  the current water content [ $L^3 L^{-3}$ ],  $\theta_s$  the saturated water content [ $L^3 L^{-3}$ ],  $H = h + z$  the equivalent freshwater head [L],  $h = \frac{P}{\rho_0 g}$  the pressure head,  $P$  the pressure [Pa],  $z$  the upward vertical coordinate [L],  $t$  the time [T],  $\mathbf{q}$  the Darcy's velocity [ $LT^{-1}$ ],  $q_s$  the sink term [ $T^{-1}$ ],  $k_r$  the relative conductivity [-],

$\mathbf{K} = \frac{\rho_0 g}{\mu} \mathbf{k}$  the hydraulic conductivity tensor [ $\text{LT}^{-1}$ ],  $\rho_0$  the density of the displaced fluid [ $\text{ML}^{-3}$ ],  $g$  the gravity acceleration [ $\text{LT}^{-2}$ ],  $\mu$  the fluid dynamic viscosity [ $\text{ML}^{-1}\text{T}^{-1}$ ],  $\mathbf{k}$  the permeability tensor dependent only on the porous medium [ $\text{L}^2$ ], and  $\rho$  the fluid density [ $\text{ML}^{-3}$ ].

The solute transport in the unsaturated zone is ruled by the advection-dispersion equation:

$$\frac{\partial(\theta C)}{\partial t} + \nabla \cdot (\mathbf{q}C) - \nabla \cdot (\mathbf{D}\nabla C) = q_s C \quad (3)$$

where  $C$  [-] is the scaled concentration and  $\mathbf{D}$  the dispersion tensor given by:

$$\mathbf{D} = D_m \mathbf{I} + (\alpha_L - \alpha_T) \mathbf{q} \otimes \mathbf{q} / |\mathbf{q}| + \alpha_T |\mathbf{q}| \mathbf{I} \quad (4)$$

with  $\alpha_L$  and  $\alpha_T$  the longitudinal and transverse dispersivities [L],  $D_m$  the pore water diffusion coefficient [ $\text{L}^2\text{T}^{-1}$ ], and  $\mathbf{I}$  the unit tensor.

We use the standard van Genuchten (1980) model to define the relation between water content and pressure head:

$$S_e = \frac{\theta(h) - \theta_r}{\theta_s - \theta_r} = \begin{cases} \frac{1}{(1 + (\alpha|h|)^n)^m} & h < 0 \\ 1 & h \geq 0 \end{cases} \quad (5)$$

where  $\alpha$  [ $\text{L}^{-1}$ ] and  $n$  [-] are the van Genuchten parameters,  $m = 1 - 1/n$ ,  $S_e$  [-] the effective saturation, and  $\theta_r$  the residual water content [ $\text{L}^3\text{L}^{-3}$ ].

The conductivity-saturation relationship is analytically derived from the Mualem (1976) model, as proposed by van Genuchten (1980):

$$k_r = S_e^{1/2} \left[ 1 - (1 - S_e^{1/m})^m \right]^2 \quad (6)$$

$$\sum_j N_{ij}^E \left( TH_j^E + \frac{\rho_E - \rho_0 z_j^E}{\rho_0} \right) + \sum_j N_{ij}^{E'} \left( TH_j^{E'} + \frac{\rho_{E'} - \rho_0 z_j^{E'}}{\rho_0} \right) - \left( \frac{|E|}{3} r_E + \frac{|E'|}{3} r_{E'} \right) \frac{dTH_i^E}{dt} + \frac{Q_S^E}{3} + \frac{Q_S^{E'}}{3} = 0 \quad (10)$$

Darcy velocity  $\mathbf{q}$  in Eq. (2) depends on both the pressure head  $h$  and the concentration  $C$ .

The flow and transport equations are coupled by the state equations. In the case of salt contamination, we can use the polynomial approximations given in Diersch and Kolditz (2002):

$$\rho = \rho_0 + (\rho_1 - \rho_0)C, \quad \text{and} \quad \mu = \mu_0 (1.0 + 0.4819C - 0.2774C^2 + 0.7814C^3) \quad (7)$$

where  $\rho_0$  and  $\rho_1$  are densities of freshwater and saltwater and  $\mu_0$  the freshwater viscosity. Different state equations may be used for density or viscosity (Diersch and Kolditz, 2002).

### 3. The numerical model

The system of nonlinear Eqs. (1)–(7), valid in 3D domains, is solved hereafter for 2D vertical domains using adapted advanced numerical methods that allow an accurate estimation of the velocity and concentration distributions for heterogeneous domains and unstructured meshes. The main stages to form the final system to be solved are summarized hereafter for a general triangular mesh.

#### 3.1. The lumped MHFE method for modeling fluid flow

With the classical standard FE method, the head is approximated linearly inside each element using standard chapeau functions, and hence, the velocity is constant at the element level. With the MHFE

method, we assume a linear approximation for the velocity  $\mathbf{q}$  inside each triangle  $E$  using the linear Raviart-Thomas basis functions:

$$\mathbf{q} = \sum_{j=1}^3 Q_j^E \mathbf{w}_j^E \quad (8)$$

where  $Q_j^E$  is the flux across the edge  $j$  of  $E$  and  $\mathbf{w}_j^E$  is the Raviart-Thomas basis function (Raviart and Thomas, 1977).

The mass lumping procedure is used to avoid over- and undershoots observed for transient simulations with small time steps (Younes et al., 2006; Belfort et al., 2009). The basic idea of this procedure is to consider steady-state flow (the mean head at the element  $E$  is  $H_E = (TH_1^E + TH_2^E + TH_3^E)/3$ ), and then the transient component is directly added to the expression of the flux (Ackerer and Younes, 2008):

$$Q_i^E = \sum_j N_{ij}^E \left( TH_j^E + \frac{\rho_E - \rho_0 z_j^E}{\rho_0} \right) - \frac{|E|}{3} r_E \frac{dTH_i^E}{dt} + \frac{Q_S^E}{3} \quad (9)$$

where  $TH_i^E$  (resp.  $z_i^E$ ) is the mean head (resp. mean elevation) of the edge  $i$  of  $E$  with  $TH_i = Th_i + z_i$ ,  $Th_i$  is the mean pressure head,  $j$  is an edge of  $E$ ,  $N$  is a local matrix of coefficients  $N_{ij}^E = -k_r^E \frac{\det(\mathbf{K}_E)}{|E|} \mathbf{r}_i^T \cdot \mathbf{K}_E^{-1} \cdot \mathbf{r}_j$  where  $\mathbf{r}_i$  is the edge vector face to the vertex  $i$  of the element  $E$  (see Younes et al. (2004) for more details),  $|E|$  is the area of  $E$ ,  $r_E = c(h_E) + S_S \theta(h_E) / \theta_S$  is the accumulation term in Richards' equation,  $h_E$  is the mean pressure head at  $E$ , and  $Q_S^E = \int_E q_S$  is the sink term on  $E$ .

The final flow system is formed by imposing continuity of heads ( $TH_i^E = TH_i^{E'}$ ) and fluxes ( $Q_i^E + Q_i^{E'} = 0$ ) between the adjacent elements  $E$  and  $E'$  having a common edge  $i$ :

The indices  $i$  and  $j$  are global, and the system is solved for the mean heads at edges  $TH_i$ .

In the case of a Dirichlet condition with a prescribed head  $H_{imp}$  at the boundary edge  $i$ , Eq. (10) is replaced by  $TH_i = H_{imp}$ . If the boundary edge  $i$  has a prescribed flux  $Q_{imp}$  (Neumann boundary condition), Eq. (10) is replaced by  $Q_i^E + Q_{imp} = 0$ .

Note that the system of Eqs. (10) is highly nonlinear since (i) the local matrix  $N$  and the accumulation term  $r$  depend on the pressure head and (ii) the hydraulic conductivity and the buoyancy term depend on the concentration.

#### THE DG-MPFA METHOD FOR MODELING SOLUTE TRANSPORT

Using the mass conservation of the fluid, given by Eq. (1), the transport Eq. (3) simplifies to:

$$\theta \frac{\partial C}{\partial t} + \mathbf{q} \nabla C + \nabla \cdot \mathbf{q}_D = 0. \quad (11)$$

With  $\mathbf{q}_D = -\mathbf{D}\nabla C$ , the dispersive flux, assumed to have a constant divergence over the element  $E$ :

$$\nabla \cdot \mathbf{q}_D = \frac{1}{|E|} \sum_i Q_d^E \quad (12)$$

where  $Q_d^E$  is the dispersive flux across the edge  $i$  of  $E$ .

The concentration inside the element  $E$  is approximated with linear discontinuous functions:

$$C^E = \sum_{i=1}^3 C_{E,i} \phi_{E,i} \tag{13}$$

with  $\phi_{E,i}$  being the interpolation function and  $i$  a local index that refers to the  $i$ th DOF  $C_{E,i}$  of the concentration inside the element  $E$ .

In the literature, the DOFs are often chosen (see, for instance, (Moortgat and Firoozabadi, 2016)) to be the concentration at the nodes and  $\phi_{E,i}$  the classical chapeau functions. In this work, the DOFs are the mean concentration  $C_{E,1}$  and the components of the concentration gradient  $C_{E,2}$  and  $C_{E,3}$ , with the corresponding interpolation functions:

$$\phi_{E,1} = 1, \quad \phi_{E,2} = (x - x_E), \quad \phi_{E,3} = (z - z_E),$$

where  $x$  and  $z$  are horizontal and vertical coordinates, and  $x_E$  and  $z_E$  are the coordinates of the center of the element  $E$ . Thus, the polynomial approximation of the concentration inside the element  $E$  is  $C^E = C_{E,1} + C_{E,2}(x - x_E) + C_{E,3}(z - z_E)$ .

The variational formulation of Eq. (11) using the test function  $\phi_{E,i}$  is:

$$\int_E \theta \frac{\partial C}{\partial t} \phi_{E,i} - \int_E C \nabla \cdot (\mathbf{q} \phi_{E,i}) + \int_E \nabla \cdot (\mathbf{q} C \phi_{E,i}) + \int_E \phi_{E,i} \nabla \cdot \mathbf{q}_D = 0 \tag{14}$$

Using Green's formula and Eqs. (12) and (13), we obtain:

$$\sum_j \frac{dC_{E,j}}{dt} \theta_E \int_E \phi_{E,j} \phi_{E,i} - \sum_j \int_E C_{E,j} \phi_{E,j} \nabla \cdot (\mathbf{q} \phi_{E,i}) + \sum_j \int_E C_j^* \phi_{E,i} \mathbf{q} \cdot \boldsymbol{\eta}_j^E + \sum_j Qd_j^E \int_E \phi_{E,i} = 0 \tag{15}$$

where  $C_j^*$  is the upstream concentration at the edge  $j$ ,  $\boldsymbol{\eta}_j^E$  is the unit outward normal vector to the edge  $j$  of  $E$ , and  $\mathbf{q}$  is the velocity obtained by substituting Eq. (9) into Eq. (8).

Eq. (15) is written for the three test functions  $\phi_{E,i}$  ( $i = 1, 2, 3$ ) for each element  $E$ . The index  $j$  ( $j = 1, 2, 3$ ) refers to the  $j^{\text{th}}$  DOF of the concentration in the element  $E$  in the two first terms of Eq (15) and to the  $j^{\text{th}}$  edge of  $E$  for the last two terms in Eq. (15).

The upstream concentration  $C_j^*$  at the edge  $j$  can be written as follows:

$$C_j^* = \tau_j^E C_j^E + (1 - \tau_j^E) C_j^E \tag{16}$$

with  $\tau_j^E = 1$  for an outward flux ( $\mathbf{q} \cdot \boldsymbol{\eta}_j^E \geq 0$ ), else  $\tau_j^E = 0$ .

Thus,  $C_j^*$  corresponds to  $C_j^E$ , the concentration at the edge  $j$  calculated using the polynomial approximation of the concentration at the element  $E$ , or  $C_j^E$ , the concentration at  $j$  calculated using the polynomial approximation of the concentration at the element  $E'$ , sharing the edge  $j$  with  $E$ .

Eq. (15) yields three equations for each element  $E$  having 3 adjacent elements ( $E1, E2, E3$ ):

$$[A] \begin{pmatrix} \frac{dC_{E,1}}{dt} \\ \frac{dC_{E,2}}{dt} \\ \frac{dC_{E,3}}{dt} \end{pmatrix} = [B] \begin{bmatrix} C_{E,1} \\ C_{E,2} \\ C_{E,3} \end{bmatrix} - [M^0] \begin{bmatrix} C_{E,1} \\ C_{E,2} \\ C_{E,3} \end{bmatrix} - \sum_{\ell=1}^3 [M^\ell] \begin{bmatrix} C_{E\ell,1} \\ C_{E\ell,2} \\ C_{E\ell,3} \end{bmatrix} - \begin{bmatrix} \sum_j Qd_j^E \\ 0 \\ 0 \end{bmatrix} \tag{17}$$

with:

$$A_{ij} = \theta_E \int_E \phi_{E,j} \phi_{E,i} \quad B_{ij} = \int_E \phi_{E,j} \nabla \cdot (\mathbf{q} \phi_{E,i})$$

$$M_{ij}^0 = \sum_{\ell} \tau_{\ell}^E \mathbf{q} \cdot \boldsymbol{\eta}_{\ell}^E \int_E \phi_{E,i} \phi_{E,j} \quad M_{ij}^{\ell} = (1 - \tau_{\ell}^E) \mathbf{q} \cdot \boldsymbol{\eta}_{\ell}^E \int_E \phi_{E,i} \phi_{E\ell,j}$$

To avoid operator splitting between advection and dispersion, the dispersive flux  $Qd_j^E$  in Eq. (17) is approximated using the MPFA method. The latter has similar properties to the MFE method since both are locally conservative and can handle unstructured meshes and anisotropic and heterogeneous domains. The two methods can be equivalent for some specific situations (Younes and Fontaine, 2008; Vohraik, 2006). However, contrary to the MHFE method, which uses the concentration at the edges as DOFs, MPFA uses the mean concentration at each element as DOFs. Hence, the discrete approximation of  $Qd_j^E$  can be directly added to the system of Eq. (17), which avoids the necessary operator splitting if the MHFE method is used for dispersion, as in Siegel et al. (1997).

To calculate  $Qd_j^E$  with the MPFA method, we assume that the concentration inside the sub-cell ( $O, F_1, G, F_2$ ) formed by the node  $O$ , the center  $G$ , and the mid-edges  $F_1$  and  $F_2$  (gray area in the Fig. 1) is linear.

Hence, it can be approximated using  $C_{E,1}$ ,  $\lambda_1$  and  $\lambda_2$  the concentrations at respectively  $G$  and the two continuity points  $f_1$  and  $f_2$  located at  $\frac{Of_1}{OF_1} = \frac{Of_2}{OF_2} = \frac{2}{3}$ .

Therefore, ( $O, f_1, G, f_2$ ) is a parallelogram, and the half-edge fluxes

$$(Qd_o^1 = \int_{O, f_1} -D\nabla C \text{ and } Qd_o^2 = \int_{O, f_2} -D\nabla C) \text{ are}$$

$$\begin{pmatrix} Qd_o^1 \\ Qd_o^2 \end{pmatrix} = \frac{3}{|E|} \begin{pmatrix} -\overrightarrow{OF_1}^\perp \cdot \mathbf{D}_E \cdot \overrightarrow{OF_1}^\perp & \overrightarrow{OF_1}^\perp \cdot \mathbf{D}_E \cdot \overrightarrow{OF_2}^\perp \\ \overrightarrow{OF_1}^\perp \cdot \mathbf{D}_E \cdot \overrightarrow{OF_2}^\perp & -\overrightarrow{OF_2}^\perp \cdot \mathbf{D}_E \cdot \overrightarrow{OF_2}^\perp \end{pmatrix} \begin{pmatrix} \lambda_1 - C_{E,1} \\ \lambda_2 - C_{E,1} \end{pmatrix} \tag{18}$$

where  $\mathbf{D}_E$  is the dispersion tensor of the element  $E$ , given by Eq. (4) and using the velocity at the center of  $E$  from Eqs. (8) and (9).

Eq. (18) is written for all elements sharing the vertex  $O$ . Then, imposing continuity of half-edge fluxes and continuity of the concentration at the continuity points gives a local system, which we invert to

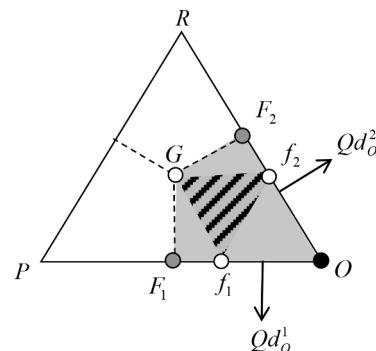


Fig. 1. A triangular element divided into three subcells, with linear concentration approximation on each subcell.

obtain explicitly the concentration at each continuity point as a function of the concentration at all elements sharing the node  $O$ . The latter is then replaced in Eq. (18), and the summation of all half-edge fluxes is then substituted into Eq. (17) (see Younes and Ackerer 2008 for more details). Therefore, the first line of the system (17) contains the contribution of all elements sharing at least one node of the element  $E$ . The second and third equations of (17) contain the contribution of adjacent elements sharing an edge with  $E$ . Note that, because of the judicious choice of DOFs, the DG\_MPFA scheme reduces to an upwind FV\_MPFA scheme by removing the second and third equations of (17) for all mesh elements.

The final vector of residuals for the global flow-transport nonlinear system is formed by the system of Eq. (10), written for the unknown pressure head  $TH_i$  at the edges, followed by the system of Eq. (17), written for the three unknown DOFs of the concentration at each element.

### 3.2. The temporal discretization

The coupled nonlinear flow Eq. (10) and transport Eq. (17) are written in a single implicit system of ordinary differential equations (ODEs) or differential algebraic equations (DAEs) of the general form:

$$F(t, y, y') = 0 \quad (19)$$

where  $y = [(TH_i)_{i=1, \dots, nb\_edges}, (C_{E,1}, C_{E,2}, C_{E,3})_{E=1, \dots, nb\_elements}]$  is the vector of unknowns formed by (i) the head traces at all the edges of the mesh (except Dirichlet boundary edges) and (ii) the three DOFs for the concentration at each element of the mesh. This vector reduces to  $y = [(TH_i)_{i=1, \dots, nb\_edges}, (C_{E,1})_{E=1, \dots, nb\_elements}]$  with only one DOF per element for the concentration in the case of FV (instead of DG) formulation.

The system (19) is solved in time using higher-order methods, which are known to be more efficient than lowest-order methods. Indeed, higher-order methods allow larger time steps and less effort in the nonlinear solver compared with the lowest-order methods (Farthing et al., 2002). Furthermore, higher-order methods are often combined with an efficient automatic time-stepping scheme, which improves the computational efficiency. The time-step size management is optimized to maintain a given temporal discretization error (Fahs et al., 2009; Farthing et al., 2002; Tocci et al., 1997; Kavetski et al., 2001).

Among the integration methods, the Backward Difference Formula (BDF) has good stability properties and is well adapted for time integration of stiff problems (Kees and Miller, 2002). The Fixed Leading Coefficient Backward Difference Formula (FLCBDF) is used in this work via the DASPK solver. The basic idea of the  $k$ th-order FLCBDF method is to convert the system  $F(t_n, y_n, y'_n) = 0$  at a given time  $t_n = t_{n-1} + \underline{h}$  with solution history  $y_{n-1}, \dots, y_{n-k}$  to the system  $F(t_n, y_n, \hat{a}y_n + \hat{b}) = 0$  where  $\hat{a}$  and  $\hat{b}$  depend on the step size  $\underline{h}$ , the order  $k$ , and the solution history (see Brennan et al. 1996 for more details).

The main advantages of the FLCBDF method are: (i) it avoids the unstable behavior of the interpolated fixed-step methods and (ii) the Newton iteration matrix can be reused for more steps than in a fully variable-step approach (Van Keken et al., 1995; Hindmarsh and Petzold, 1995).

The Jacobian matrix is evaluated numerically using finite difference approximation. The same Jacobian matrix is used for several time steps to improve efficiency. Furthermore, to reduce drastically the computational time required for the calculation of the Jacobian, sparsity and structure of  $J$  are provided and the variables are perturbed by group using the column grouping technique (see Curtis et al. 1974, Hindmarsh 1982).

The order (up to the fifth-order) of BDF, as well as the time step's size, are optimized to reduce the computational effort while maintaining a small temporal truncation error. The latter is estimated using a predictor-corrector scheme. Both absolute and relative convergence criteria are fixed to  $10^{-5}$  in this work.

In this work, we use the DASPK time solver with the preconditioned Krylov iterative method to solve the linear systems arising at each time step.

## 4. Numerical experiments

Three test cases are investigated to show the efficiency and accuracy of the developed numerical model. The first test case is inspired by the laboratory experiment performed by Vauclin et al. (1979). It deals with the infiltration, under constant flux, of a dense contaminant into an unsaturated-saturated porous medium. This test, which is relatively simple from a computational point of view, is used to validate the developed code against a standard finite element solution obtained using COMSOL Multiphysics®. The second test case, inspired by the work of Forsyth and Kropinski (1997), deals with the infiltration of a dense contaminant in a heterogeneous initially dry soil. The simulated moving sharp front induces high nonlinearity, which makes this computational test cases very challenging. It is used to highlight the efficiency of our newly developed model and to assess the advantages of combining high-performance numerical methods compared with classical ones implemented in COMSOL. The last test case is investigated to show the applicability of the new model to large-scale problems. In this test case, the developed numerical tool is used to simulate a simplified conceptual 2D model of saltwater intrusion under climate change for the Akkar coastal aquifer in Lebanon.

### 4.1. Infiltration of a dense contaminant in an unsaturated-saturated porous medium

Vauclin et al. (1979) performed laboratory experiments to investigate the transient position of the water table under artificial recharge. The problem is extended here by including the infiltration from the surface of a dense contaminant and used for the validation of the new model by comparison with COMSOL results. The domain is a rectangular sandbox of  $600 \times 200$  cm, with the water table located at 65 cm from the bottom. The initial conditions correspond to hydrostatic pressure distribution with a domain free from pollutants. Infiltration of a contaminant under a constant flux of 86.4 cm/day is then applied over 200 cm in the center of the soil surface. A Dirichlet boundary condition with a head of 65 cm is fixed below the water table. A no-flow boundary is prescribed for the bottom and top surface, except for the infiltration zone. Owing to the symmetry of this problem, only the right-hand side of the domain is modeled with a no-flow boundary imposed along the axis of symmetry. The material properties are given in Table 1.

The simulation is performed for 80 h using a triangular mesh formed by 4273 triangular elements. Two configurations are investigated: in the first one, the injected contaminant is a tracer ( $\rho_1 = 1000 \text{ kg/m}^3$ ), whereas in the second, the contaminant has a higher density ( $\rho_1 = 1100 \text{ kg/m}^3$ ).

**Table 1**  
Simulation parameters for the first test case inspired from Vauclin et al. (1979).

Parameters	
$\theta_r$	0.01
$\theta_s$	0.3
$\alpha(\text{cm}^{-1})$	0.033
$n$	4.1
$K(\text{cm.s}^{-1})$	$10^{-2}$
$S_s(\text{cm}^{-1})$	$10^{-10}$
$\alpha_l(\text{cm})$	1
$\alpha_T(\text{cm})$	0.1
$D_m(\text{m}^2/\text{s})$	$10^{-9}$
$\rho_0(\text{kg/m}^3)$	1000
$\rho_1(\text{kg/m}^3)$	1000 or 1100
$\mu(\text{kgm}^{-1}\text{s}^{-1})$	0.001

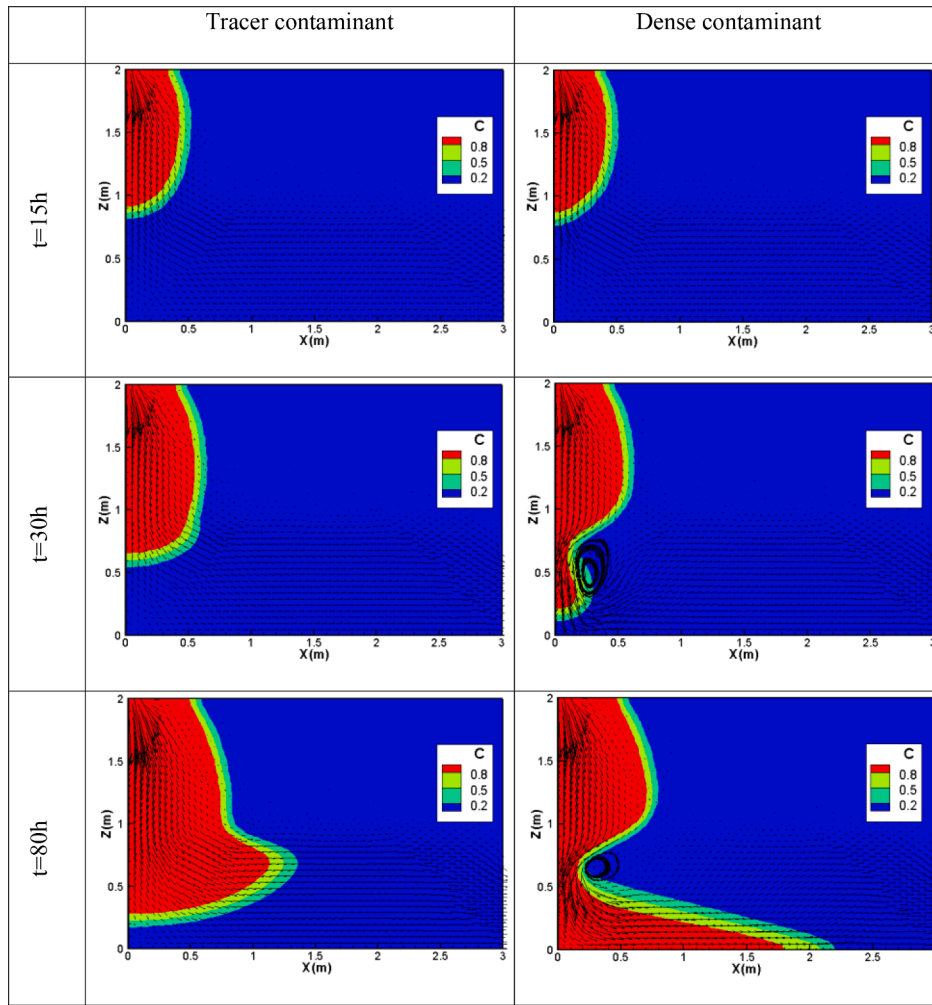


Fig. 2. velocity field and contaminant distributions for the infiltration of a tracer and a dense contaminant in an unsaturated-saturated system.

The evolution of the contaminant plume during the time for both situations is shown in Fig. 2. Before reaching the water table (initially at  $z = 65$  cm), the tracer and dense contaminant plumes are almost the same (see results at  $t = 15$  h). Indeed, density variation seems to have no effect during the transport through the unsaturated zone. The main reasons for this similarity are that (i) a fixed flux is used at the surface and hence the same quantity of contaminant is intruded in the system for both situations and (ii) the density variation in the liquid phase (10%) is much less important than the density variation between the liquid and air phase, which is about three orders of magnitude. This last reason is no longer valid once the plume reaches the water table. As a consequence, due to density effects, the dense contaminant moves downward in the saturated domain, creating a recirculation zone (vortex) near the water table interface (see results of Fig. 2, at  $t = 30$  h), whereas the tracer contaminant remains near the water table. The velocity distribution in the unsaturated zone is quite similar for the tracer and dense contaminant situations, whereas strong differences can be observed in the saturated zone. For the tracer contamination, the velocity is not affected by the evolution of the contaminant and remains mainly horizontal. However, in the case of the dense contaminant, strong vertical velocities appear due to density effects, which bring the contaminant down to the bottom. As a consequence, the results in terms of velocity field and contaminant distribution at  $t = 80$  h for the dense and tracer situations are completely different. The tracer moves mainly horizontally at the upper part of the saturated zone with a maximum displacement near the water table, whereas the dense contaminant moves toward the substratum and then horizontally in the lower part of the domain. The

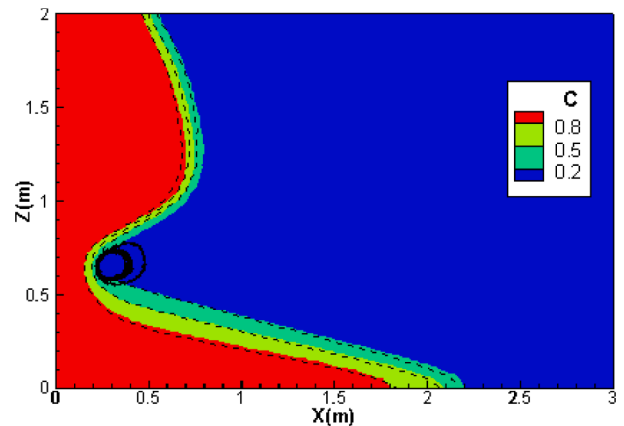


Fig. 3. Concentration distribution at  $t = 80$  h for the dense contaminant infiltration: Results of the new model (contours) versus COMSOL results (dashed-lines).

vortex remains near the water table interface (see results of Fig. 2 at  $t = 80$  h).

The validity of the new model is investigated by comparing the obtained results against those of the popular COMSOL model. The same spatial discretization was used to allow for a comparison between COMSOL and our newly developed model, and the solution was also

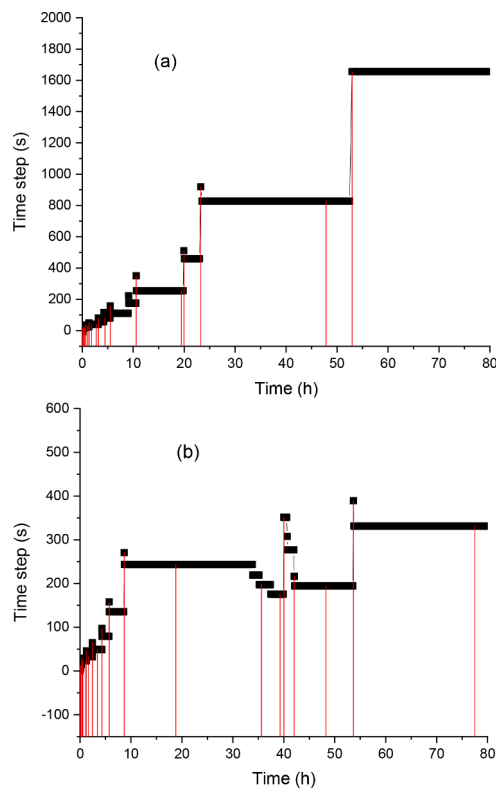


Fig. 4. Time step evolution for the tracer (a) and dense (b) contaminant infiltration simulated with the new model.

checked on a fine mesh since no analytical solution is available. The results of the two models are almost similar, which demonstrates the validity of the developed model (Fig. 3). Notice that the non-dimensional mass injected from the upper boundary during the simulation is 0.288. With the new numerical model, the total mass in the domain at 80 h is 0.28815, whereas it is 0.2820 with COMSOL. Hence, the mass balance error with COMSOL is around 0.021, whereas it is around  $5 \times 10^{-4}$  with the new model. Therefore, the very small difference observed in Fig. 3 between the isocontour levels of the new model and COMSOL is probably due to the loss of mass observed with COMSOL.

Both COMSOL and the new model were used with the MOL and a variable high-order (up to 5) time integration BDF method. The evolution of the time step's length with the new model during the simulation of the tracer and the dense contaminant infiltration situations are depicted in Fig. 4. The tracer simulation required 51 s of CPU time, for a total number of 1128 time steps. The time step starts at  $10^{-4}$  s and increases to 1655 s in almost a monotonic way (see Fig. 4a). Only 37 Jacobian evaluations are required during the 1128 time steps. The simulation of the dense contaminant required more CPU time (70 s) and needed more time steps (1751). In this case, smaller time steps are used (the maximum is 389 s), and the time step size is no longer monotonic (Fig. 4b), probably because of the more complex occurring physics. Note that the evolution of the time step's size remains quite similar before the wetting front reaches the saturated zone. The same Jacobian is maintained for several time steps since the number of evaluations of the Jacobian remains small (only 40 evaluations), which shows the efficiency of the new model.

As a comparison, the simulation of the dense contaminant with COMSOL requires 1452 time steps. The evolutions of the time step's length with both models are similar. However, the new model was around 10 times more efficient than COMSOL. Indeed, the new model spent only 70 s of CPU time, whereas COMSOL required 720 s for the whole simulation. In fact, COMSOL was very slow in the early stages of

Table 2

Simulation parameters for the problem of contaminant infiltration in a heterogeneous initial dry soil.

Parameters	Upper Layer	Lower Layer
$\theta_r$	0.0001	0.045
$\theta_s$	0.40	0.43
$\alpha(cm^{-1})$	0.0174	0.145
$n$	1.37	2.68
$K(\times 10^{-4}cm.s^{-1})$	3.5	82.5
$S_s(\times 10^{-10}cm^{-1})$	1	1
$\alpha_l(cm)$	0.5	0.5
$\alpha_r(cm)$	0.1	0.1
$D_m(m^2/s)$	$10^{-9}$	$10^{-9}$
$\rho_0(kg/m^3)$	1000	1000
$\rho_1(kg/m^3)$	1025	1025
$\mu(kgm^{-1}s^{-1})$	0.001	0.001

simulation, probably due to the significant oscillating pressure and concentration values observed in the neighborhood of the infiltration front. These unphysical oscillations affect the convergence of the nonlinear solver and increase the number of nonlinear iterations per time step.

#### 4.2. Infiltration of a dense contaminant in a heterogeneous initially dry soil

Simulating infiltration into dry soils is known to be a challenging task. Indeed, for very dry conditions, the head gradient becomes extremely large at the wetting front, which can lead to large computational times and unphysical oscillations (Zha et al., 2017). To investigate the efficiency of the developed model for such situations, we simulate the infiltration problem given in (Fahs et al., 2009). The problem is inspired from Huang et al. (1996) and involves infiltration under a constant head boundary condition into a heterogeneous dry soil. The domain has a rectangular shape of 125 cm width and 230 cm depth and contains two horizontal layers. The surface layer of 40 cm thickness is formed by a clayey soil. The subsurface layer is a sandy soil of 190 cm thickness. The properties of the two soil layers are depicted in Table 2. A Dirichlet boundary condition is prescribed in the strip  $0 \leq x \leq 20$  cm at the surface with a fixed pressure head of  $-10$  cm. A fixed pressure head of  $-10^4$  cm is maintained at the bottom of the domain. The other sides are impervious. A constant initial pressure head of  $-10^4$  cm is considered for the entire domain, which corresponds to an initial water content of  $0.059 cm^3.cm^{-3}$  and  $0.045 cm^3.cm^{-3}$ , respectively, in the upper and lower layer. The infiltrated contaminant has a density of  $1025 kg.m^{-3}$ , which corresponds to seawater density. A triangular mesh of 3505 elements is used for the spatial discretization, and the final simulation time is 7 days.

The obtained pressure and concentration distributions are shown in Fig. 5. In this figure, the pressure shows a sharp front, reflecting a very high gradient caused by the dry initial conditions ( $-100$  m).

The sharp pressure front cannot be accurately simulated with COMSOL. Indeed, the simulation of this test case with COMSOL using the same mesh failed to converge because of unphysical oscillations generated near the wetting interface. Convergence problems have been also encountered when changing the initial (and bottom) conditions from  $-100$  m to  $-1$  m. The only way to obtain a convergent solution with COMSOL was to use a finer mesh of about 14,000 elements and an initial pressure head of  $-1$  m instead of  $-100$  m. And, even for such a situation, the results of COMSOL are inaccurate since the obtained pressure head is between  $-1.4$  m and  $-0.1$  m instead of  $-1$  m and  $-0.1$  m. Besides, the solution contains strong unphysical oscillations near the wetting interface (Fig. 5a). These unphysical oscillations are avoided with the new code, thanks to the used advanced numerical methods and, especially, the mass lumping procedure, which avoids unphysical oscillations in the case of transient simulations with sharp wetting fronts

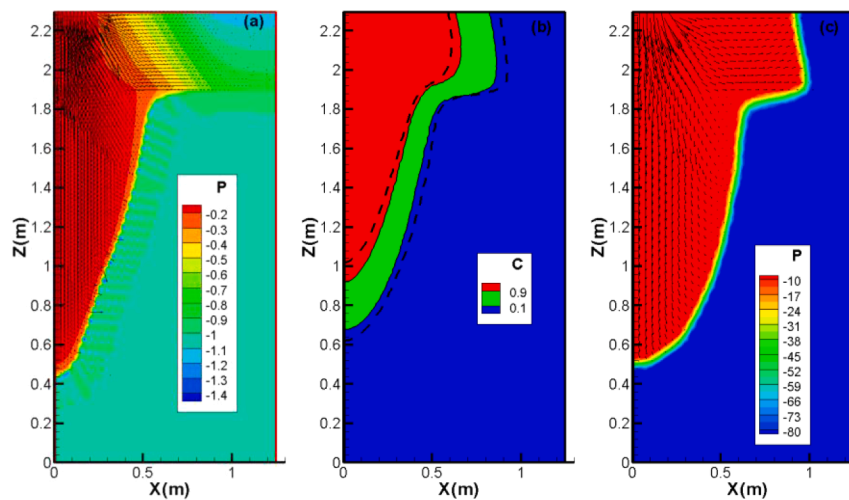


Fig. 5. (a) Pressure distribution (in m) with COMSOL, (b) pressure and (c) concentration distributions with the new model at  $t = 7$  days for the problem of contaminant infiltration in a heterogeneous initial dry soil. Dashed lines represent results of upwind first order FV instead of DG for advection.

(Younes et al., 2006; Belfort et al., 2009).

Fig. 5c shows the final concentration distribution at  $t = 7$  days. The results of a simplified version of the numerical code using the upwind first-order FV scheme instead of DG are also depicted (dashed lines) in Fig. 5c. This figure shows that a large numerical diffusion is generated using the upwind first-order FV method. To quantify the difference between the two methods, the spread of the concentration  $L_S = X_{0.9} - X_{0.1}$ , corresponding to the distance between the 10 and 90% isochlors at the left vertical side of the domain, is measured for the FV and DG simulations. The spread with FV is  $L_S^{FV} = 0.4$ , whereas with DG, it is  $L_S^{DG} = 0.24$ . Hence, due to numerical diffusion, the spread with the FV method is around 170% that of DG. This shows clearly that DG is well-adapted for advective-dominated transport and generates limited numerical diffusion compared with the upwind first-order FV method.

It is worth noting that, in the first test case, the contaminant distribution in the unsaturated region was not affected by the density of the contaminant, since the infiltration occurred under a constant flux boundary condition. For the current test case, the concentration distribution is sensitive to the density of the contaminant because of the Dirichlet boundary condition used at the surface infiltration boundary (results are not shown in the paper). The pollutant infiltration is slightly more pronounced with the dense contaminant than with the tracer contaminant. The total mass in the system at  $t = 7$  days is 0.64 kg with the tracer, whereas it is 0.66 kg if the contaminant has a density of 1025  $\text{kg}\cdot\text{m}^{-3}$ . This total mass can increase up to 0.76 kg in the case of a contaminant with a density of 1200  $\text{kg}\cdot\text{m}^{-3}$  (brine contamination).

Finally, to highlight the benefit of the higher-order time integration for the investigated challenging infiltration problem, we compare the efficiency of the model when used with a first-order and with a variable high-order (up to 5) time integration with the BDF method.

The results of Table 3 show that the high-order method requires more Jacobian evaluations, but allows much larger time steps and needs fewer calculations compared with the classical first-order method. The variable high-order method is around 7 times more efficient than the first-

Table 3

Performance statistics for the first-order and variable order methods implemented in the advanced developed model for the simulation of the second test case.

Time integration method	CPU	Nb time steps	Nb Jacobian	Max time step	Mean time step
First-order	896	28,871	115	45	21
Variable-order (up to 5)	128	4322	138	378	140

order method for the investigated problem.

### 4.3. Large-scale simulation of SWI under climate change

The developed numerical tool is used to simulate a large-scale contamination problem with large spatial and temporal ranges that occurs in the Akkar unconfined coastal aquifer, located in the north of Lebanon (Fig. 6a). The plain is cultivated with market gardening and cereals crops and the aquifer underwent a significant increase in pumping water, both for irrigation and domestic consumption, notably because of the massive arrival of Syrian refugees in the region. As a consequence, some pumping wells suffer from salinization caused by the overexploitation of the aquifer.

Because of the lack of data (infiltration rates, piezometric heads, etc.) and of precise knowledge of initial and boundary conditions, a full 3D simulation of the above-described problem has not been considered. A representative 2D vertical cross-section is designed to investigate salt-water intrusion under climate change projection and long-term pumping regimes.

The shore-perpendicular section has an extension of 2 km offshore and 6 km onshore (United Nations Development Program, 2014). The depth of the Akkar basin varies between 100 m and 170 m from the surface and is formed by fluvial deposits. In the conceptual model (Fig. 6b), the permeability field was generated assuming a lognormal distribution with a variance of 1.0  $\text{m}^4$  and a geometric average conductivity of 0.945  $10^{-11} \text{m}^2$ . An exponential correlation function was used with horizontal and vertical correlation lengths of 1000 m and 10 m, respectively. The bottom is formed by clays and marls and is considered impermeable. The left vertical side corresponds to the sea boundary, which has a prescribed concentration of  $C = 35 \text{g}\cdot\text{l}^{-1}$  and a vertical hydrostatic pressure distribution. The parameters (soil and fluid properties) used in the simulations are given in (Table 4). The recharge, depicted in Fig. 6c, corresponds to observed data for the period between 1962 and 2020 and a projection for the period 2020–2099, obtained from the IPSL\_CM5 Global Climate Model (GCM) (Van Vuuren et al., 2011). A weak regional flow is assumed at the right land boundary. Although radial upconing around wells have necessarily 3D configurations, two wells are assumed to represent the different pumping activities in the Akkar aquifer (FAO 1970). The wells are located at, respectively, 1500 m and 3000 m from the shoreline at, respectively, a depth of 45 m and 30 m. The rates for the two pumping wells (Fig. 6d) are assumed to represent the observed rates for the period 1962–2020 and expected rates (with increasing water demand) for 2020–2099. Note that pumping was stopped for Well 1 (the closest to the sea) in 2020

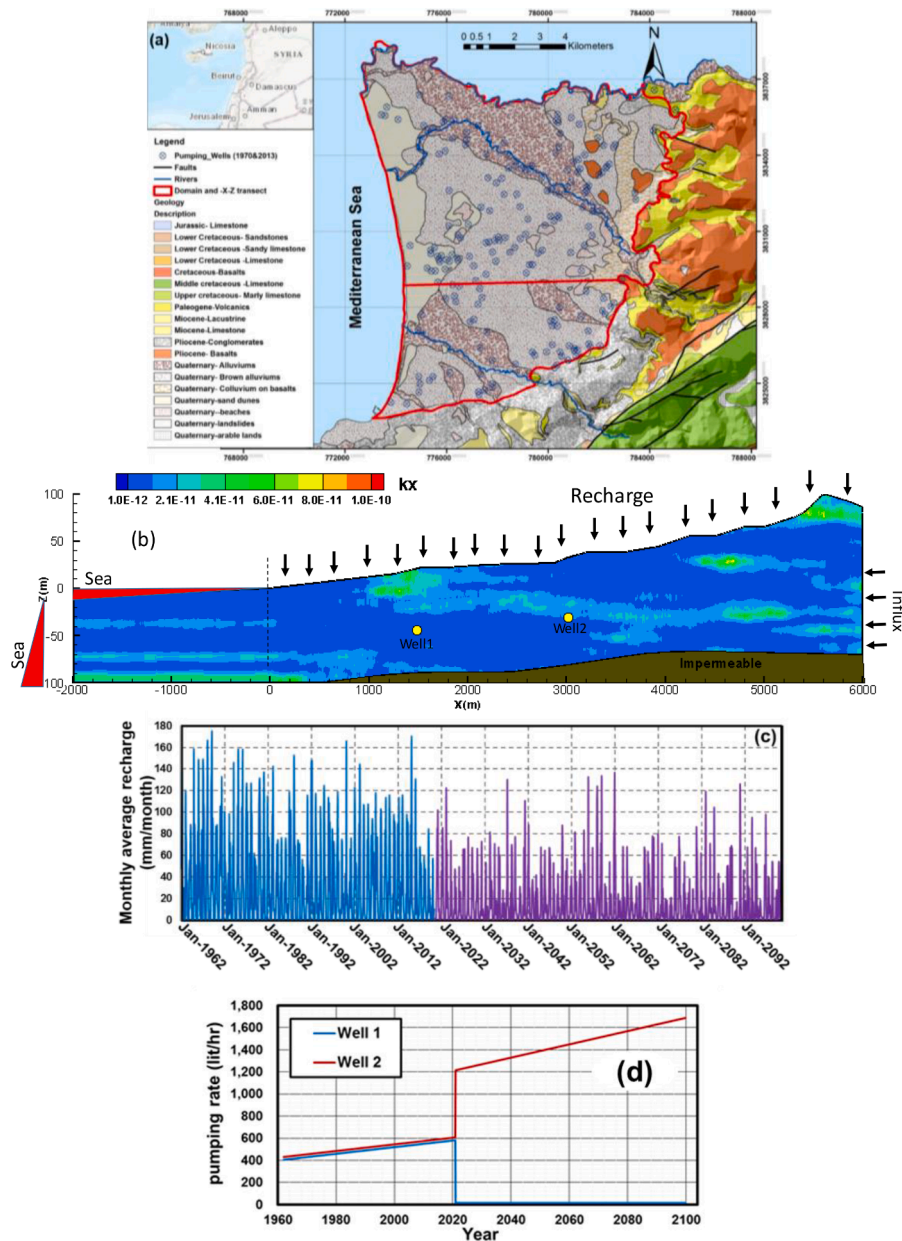


Fig. 6. (a) Location of the Akkar aquifer, (b) conceptual representation of the aquifer with a lognormal permeability field and the boundary conditions (c) the recharge data until 2019 and projections under climate change between 2020 and 2099 and (d) pumping rates in production wells.

because of salinization. The pumping rate of Well 1 was transferred to Well 2.

The domain is discretized with approximately 75 K triangular elements with an almost equal area of 15 m<sup>2</sup>. The simulation is, at first, performed for a long time with the yearly average recharge of pre-1962, without pumping to mimic the natural equilibrium conditions (Fig. 7a). The value of recharge for this period is taken uniformly and equal to 90 mm.y<sup>-1</sup>. Next, two periods are simulated: (i) the 1962–2020 period, which leads to the current situation of the coastal aquifer (Fig. 7b), and (ii) the 2020–2099 period, which corresponds to the future response of the aquifer to the impact of a climate change projection and estimated pumping regime (Fig. 7c).

The problem is solved for 333,031 DOFs (unknowns) on a computer with a single Intel i7–7700 processor 3.6 GHz and 16 Go of RAM (i.e. Random Access Memory). The whole simulation (138 years) required around 9 h of CPU time.

Fig. 7a shows that, without any pumping, the natural equilibrium

situation of 1962 shows a moderate saltwater intrusion. The concentration profile shows a small dispersion. The aquifer is only contaminated near the bottom, for a distance of around 400 m from the shoreline. Because of pumping, the concentration distribution at 2020 shows a more significant saltwater intrusion. In Fig. 7b, Well 1, located 1500 m from the shoreline, is reached by salt contamination, which is in agreement with the field observations. The breakthrough curves of salt concentration at the two wells are depicted in Fig. 8. In this figure, a small inflection is observed in 2020 when pumping is stopped at Well 1. Then, the concentration continues to increase because of the advancement of the salt front caused by the pumping in Well 2. The final concentration in Well 1 is very high and reaches 30 g.l<sup>-1</sup>. Well 2, located 3000 m from the shoreline, starts to be salinized at around 2060. Then, the concentration continues to increase significantly, with a high rate of salinization, which makes the well unusable in 2070 and onward.

Fig. 7b shows that the water table slightly falls in 2020 due to pumping. The major part of the aquifer is contaminated by salt in 2100

**Table 4**

Properties of the soil and the water for the simulation of the simplified conceptual Akkar aquifer.

Parameter	Value
Freshwater density $\rho_0(kg.m^{-3})$	1,000
Seawater density $\rho_1(kg.m^{-3})$	1,025
Gravity $g(m.s^{-2})$	9.81
Viscosity $\mu(kg.m^{-1}.s^{-1})$	$10^{-3}$
Anisotropy ratio $r_k(=k_z/k_x)$	0.1
Porosity $\epsilon$	0.39
Storage coefficient $S_s(m^{-1})$	$5 \times 10^{-4}$
Molecular diffusion $D_m(m^2.s^{-1})$	$1.0 \times 10^{-9}$
$\alpha(cm^{-1})$	0.01
$n$	1.75
$\theta_s$	0.39
$\theta_r$	0.1
$\alpha_l(m)$	5
$\alpha_7(m)$	0.5
Right boundary condition: Regional flow/ unit width $q_d(m^2.s^{-1})$	$6 \times 10^{-7}$

(Fig. 7c) because of (i) the reduced recharge caused by climate change and (ii) the increase of the pumping rate of Well 2 due to the expected increase of water demand. The progress of saltwater intrusion inside the aquifer is relatively fast, as can be observed in Fig. 9, which depicts the evolution of  $L_{toe}$  (i.e. the maximum horizontal distance between the shoreline and the 50% salt concentration contour line). The evolution of  $L_{toe}$  is almost linear until 2070. The saltwater intrusion is significant and fast. From Fig. 9, the salt front invades the domain, with an almost constant velocity of  $25 m.y^{-1}$ .

Finally, note that the predicted state in 2100 (Fig. 7c) shows that a significant water table falls more than 20 m, which warrants the use of that saturated-unsaturated model to investigate problems of density-driven flow in unconfined coastal aquifers.

**5. Conclusion**

Unsaturated-saturated aquifer systems can be subject to pollution by dense contaminants such as SWI in coastal unconfined aquifers. Modeling such problems requires the solution of a highly nonlinear system combining the nonlinear Richards' equation with the advection-dispersion transport equation. The solution of such a nonlinear system

can be hampered by convergence issues and excessive computational time, especially for regional-scale problems. A new model has been developed in this work based on advanced spatial discretization

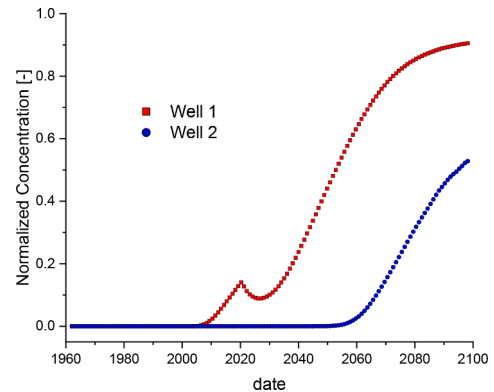


**Fig. 8.** Dimensionless concentration (concentration/seawater concentration) at the two pumping wells.

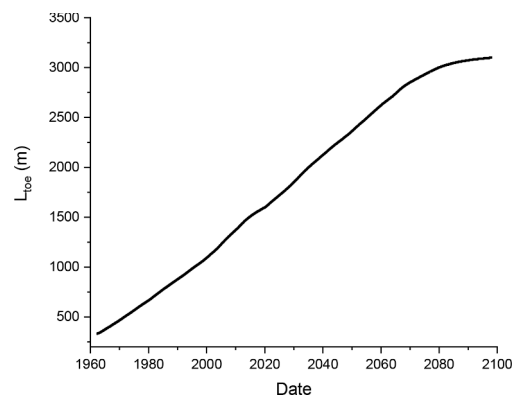


**Fig. 9.** Evolution of  $L_{toe}$  (the maximum horizontal distance between the shoreline and the 50% salt concentration contour).

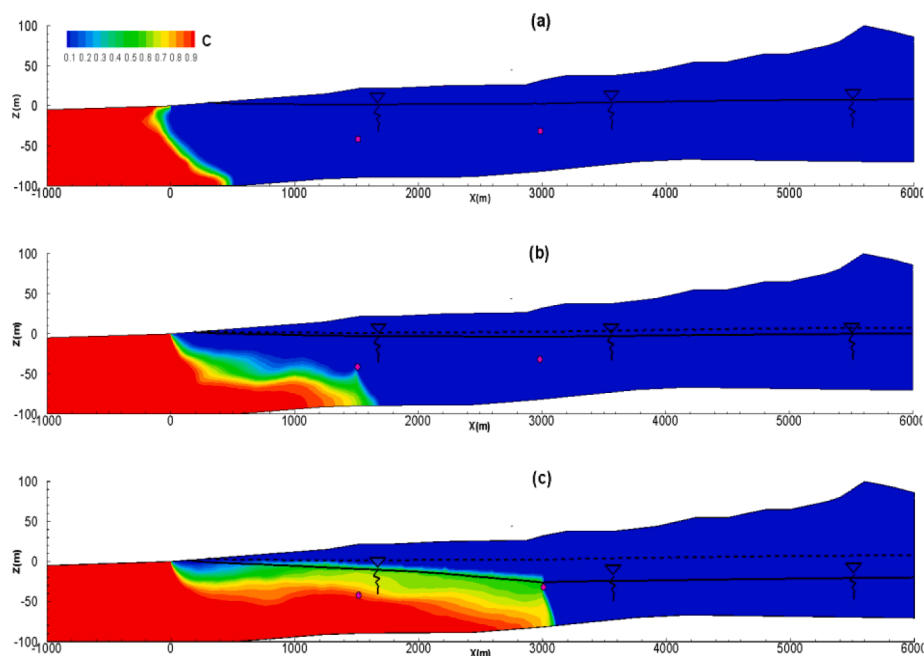


**Fig. 7.** Spatial salinity distribution in the aquifer and water table position: (a) at 1962 (state of equilibrium), (b) currently at 2020 and (c) predictions for 2099.

methods (lumped MHFE, implicit DG and MPFA methods) and higher-order time integration techniques via the method of lines.

The efficiency and accuracy of the new model have been investigated for three test cases. The first test case deals with the infiltration of a contaminant in an unsaturated-saturated rectangular sandbox. This test case served as a benchmark to validate the numerical model. The results of simulations are similar to those obtained with COMSOL. Tracer and dense contaminants yielded similar plumes in the unsaturated zone. However, when the water table is reached, the dense contaminant moves downward, creating a recirculation zone, whereas the tracer moves horizontally along the water table. The test case shows that the new model is highly efficient since it uses large time steps and maintains the same Jacobian for several calculations.

The second test case deals with the challenging problem of infiltration into a heterogeneous and initially very dry soil. For this problem, COMSOL failed to reproduce the sharp pressure front and generated strong unphysical oscillations. The new model gives accurate results, and the higher-order integration method is around 7 times more efficient than the classical first-order method.

Finally, the developed model has been used to simulate a simplified 2D conceptual model of SWI in the Akkar unconfined aquifer, under climate change and long-term pumping regimes. The purpose of this last test case was to show the applicability of the newly developed model in simulating large-scale regional problems under dynamic conditions. The results show that SWI was moderate in the case of natural equilibrium (in 1962). Then, because of the pumping undergone in the past decades, a significant SWI occurred and salinization reached the pumping well at 1500 m. Simulations until 2100 show that the reduced recharge caused by climate change and the increase in pumping due to the evolution of water demand induce significant salinization of the aquifer, with a salt front advancing inland at an average speed of  $25 \text{ m.y}^{-1}$  and an important water table fall. Note that these preliminary results must be taken with caution since the simulations were performed on a simplified 2D conceptual model without any calibration because of the lack of data.

This study points out that the newly developed numerical model is an interesting tool to assess environmental issues. Efficient and robust numerical models are useful for applications at large scales, involving repetitive simulations, as in model calibration, sensitivity/uncertainty analysis, and scenario-based studies.

#### CRedit authorship contribution statement

**Anis Younes:** Methodology, Writing – original draft. **Behshad Koohbor:** Visualization. **Benjamin Belfort:** Visualization, Writing – original draft. **Philippe Ackerer:** Supervision, Writing – review & editing. **Joanna Doummar:** Visualization. **Marwan Fahs:** Resources, Visualization.

#### Declaration of Competing Interest

The authors declare that there is no conflict of interest regarding the publication of this article.

#### Acknowledgments

The authors wish to thank the Investissements d'Avenir and ADEME for supporting this work as part of the GEOTREF research project.

Marwan Fahs would like to acknowledge the support from the National School of Water and Environmental Engineering of Strasbourg through the research project PORO6100.

#### References

Diersch, H.J., Kolditz, O., 2002. Variable-density flow and transport in porous media: approaches and challenges. *Adv. Water Resour.* 25, 899–944.  
 Simmons, C.T., 2005. Variable-density groundwater flow: from current challenges to future possibilities. *Hydrogeol. J.* 13, 116–119.

Graf, T., Simmons, C.T., Boufadel, M.C., Neuweiler, I., 2010. Movement of dense plumes in variably saturated porous media: numerical model and results. In: *Proceedings of the 18th International Conference on Water Resources (CMWR)*. Barcelona, Spain. June 2010. Abstract 23.  
 Werner, A.D., Bakker, M., Post, V.E.A., Vandenbohede, A., Lu, C., Ataie-Ashtiani, B., et al., 2013. Seawater intrusion processes, investigation and management: recent advances and future challenges. *Adv. Water Resour.* 51, 3–26.  
 Simmons, C.T., Pierini, M.L., Hutson, J.L., 2002. Laboratory investigation of variable density flow and solute transport in unsaturated-saturated porous media. *Transp. Porous Media* 47, 215–244.  
 Oostrom, M., Hayworth, J.S., Dane, J.H., Guven, O., 1992. Behaviour of dense aqueous phase leachate plumes in homogeneous porous media. *Water Resour. Res.* 28 (8), 2123–2134.  
 Dane, F.H., Guven, O., Oostrom, M., Hayworth, J.S., Leijnse, A., 1994. Dense Aqueous Phase Contaminant Plume Behavior in Porous Media Near the Groundwater Table, 222. IAHS, pp. 333–340. Publ.  
 Ouyang, Y., Zheng, C., 1999. Density-driven transport of dissolved chemicals through unsaturated soil. *Soil Sci.* 164 (6), 376–390.  
 Boufadel, M.C., Suidan, M.T., Venosa, A.D., 1999. Numerical modeling of water flow below dry salt lakes: effect of capillarity and viscosity. *J. Hydrol.* 221, 55–74.  
 America, I., Zhang, C., Werner, A.D., van der Zee Sjoerd, E.A.T.M., 2020. Evaporation and salt accumulation effects on riparian freshwater lenses. *Water Resour. Res.* 56 <https://doi.org/10.1029/2019WR026380> e2019WR026380.  
 Werner, A.D., Lockington, D.A., 2004. The potential for soil salinization above aquifers impacted by seawater intrusion. In: *Proceedings of the 13th International Soil Conservation Organisation Conference. Conserving Soil and Water for Society: Sharing Solutions*, edited by S. R. Raine et al., 6 pp., ASSSI/IECA, Brisbane.  
 Werner, A.D., Lockington, D.A., 2006. Tidal impacts on riparian salinities near estuaries. *J. Hydrol.* 328, 511–522.  
 Ibrahim, M.K., Miyazaki, T., Nishimura, T., Imoto, H., 2014. Contribution of shallow groundwater rapid fluctuation to soil salinization under arid and semiarid climate. *Arab. J. Geosci.* 7, 3901–3911.  
 Badaruddin, S., Werner, A.D., Morgan, L.K., 2015. Water table salinization due to seawater intrusion. *Water Resour. Res.* 51, 8397–8408.  
 Qu, W., Li, H., Wan, L., Wang, X., Jiang, X., 2014. Numerical simulations of steady-state salinity distribution and submarine groundwater discharges in homogeneous anisotropic coastal aquifers. *Adv. Water Resour.* 74, 318–328.  
 Zhou, P., Li, G., Lu, Y., Li, M., 2014. Numerical modeling of the effects of beach slope on water-table fluctuation in the unconfined aquifer of Donghai Island, China. *Hydrogeol. J.* 22, 383–396.  
 Ataie-Ashtiani, B., Volker, R.E., Lockington, D.A., 2001. Tidal effects on groundwater dynamics in unconfined aquifers. *Hydrol. Process* 15, 655–669.  
 Farthing, M.W., Ogden, F.L., 2017. Numerical solution of Richards' Equation: a review of advances and challenges. *Soil Sci. Soc. Am. J.* 81, 1257.  
 Szymkiewicz, A., 2013. *Modelling Water Flow in Unsaturated Porous Media*, GeoPlanet: Earth and Planetary Sciences. Springer, Berlin, Heidelberg. Berlin Heidelberg.  
 Zha, Y., Yang, J., Yin, L., Zhang, Y., Zeng, W., Shi, L., 2017. A modified Picard iteration scheme for overcoming numerical difficulties of simulating infiltration into dry soil. *J. Hydrol.* 551, 56–69.  
 Durlofsky, L., 1994. Accuracy of mixed and control volume finite element approximations to darcy velocity and related quantities. *Water Resour. Res.* 30 (4), 965–974.  
 Schneider, M., Glaser, D., Flemisch, B., Helmig, R., 2018. Comparison of finite-volume schemes for diffusion problems. *Oil Gas Sci. Technol. Rev. IFP Energ. Nouvelles* 73, 82.  
 Konz, M., Ackerer, P., Younes, A., Huggenberger, P., Zechner, E., 2009. 2D stable layered laboratory-scale experiments for testing density-coupled flow models. *Water Resour. Res.* 45, W02404.  
 Younes, A., Ackerer, P., 2010. Empirical vs. time stepping with embedded error control for density-driven flow in porous media. *Water Resour. Res.* 46 (8).  
 Chavent, G., Roberts, J.E., 1991. A unified physical presentation of mixed, mixed-hybrid finite element method and standard finite difference approximations for the determination of velocities in water flow problems. *Adv. Water Resour.* 14 (6), 329–348.  
 Younes, A., Ackerer, P., Delay, F., 2010. Mixed finite element for solving 2D diffusion-type equations. *Rev. Geophys.* 48 (1).  
 Younes, A., Ackerer, P., Lehmann, F., 2006. A new mass lumping scheme for the mixed hybrid finite element method. *Int. J. Numer. Methods Eng.* 67 (1), 89–107.  
 Belfort, B., Ramasomanan, F., Younes, A., Lehmann, F., 2009. An efficient lumped mixed hybrid finite element formulation for variably saturated groundwater flow. *Vadose Zone J.* 8, 352–362.  
 Younes, A., Ackerer, P., 2008. Solving the advection-dispersion equation with discontinuous galerkin and multipoint flux approximation methods on unstructured meshes. *Int. J. Numer. Methods Fluids* 58 (6), 687–708.  
 Siegel, P., Mosé, R., Ackerer, P., Jaffré, J., 1997. Solution of the advection-diffusion equation using a combination of discontinuous and mixed finite elements. *Int. J. Numer. Methods Fluids* 24, 595–613.  
 Ackerer, P., Younes, A., Mosé, R., 1999. Modelling variable density flow and solute transport in porous medium: 1. Numerical model and verification. *Transp. Porous Media* 35, 345–373.  
 Hoteit, H., Firoozabadi, A., 2005. Multicomponent fluid flow by discontinuous Galerkin and mixed methods in unfractured and fractured media. *Water Resour. Res.* 41 (11).  
 Aavatsmark, I., Barkve, T., Bøe, O., Mannseth, T., 1998. Discretization on unstructured grids for inhomogeneous, anisotropic media. Part I: derivation of the methods. *SIAM J. Sci. Comput.* 19 (5), 1700–1716.

- Younes, A., Fontaine, V., 2008. Hybrid and multi point formulations of the lowest order mixed methods for Darcy's Flow on triangles. *Int. J. Numer. Methods Fluids* 58 (9), 1041–1062.
- Ackerer, P., Younes, A., 2008. Efficient approximations for the simulation of density driven flow in porous media. *Adv. Water Resour.* 31 (1), 15–27.
- Fahs, M., Younes, A., Lehmann, F., 2009. An easy and efficient combination of the mixed finite element method and the method of lines for the resolution of Richards' equation. *Environ. Model. Softw.* 24 (9), 1122–1126.
- Younes, A., Fahs, M., Ahmed, S., 2009. Solving density driven flow problems with efficient spatial discretizations and higher-order time integration methods. *Adv. Water Resour.* 32 (3), 340–352.
- Van Keken, P.E., Yuen, D.A., Petzold, L.R., 1995. DASP: a new high order and adaptive time-integration technique with applications to mantle convection with strongly temperature- and pressure-dependent rheology. *Geophys. Astrophys. Fluid Dyn.* 80 (1–2), 57–74.
- van Genuchten, M.T., 1980. A closed-form equation for predicting the hydraulic conductivity of unsaturated soils. *Soil Sci. Soc. Am. J.* 44 (5), 892–898.
- Mualem, Y., 1976. A new model for predicting the hydraulic conductivity of unsaturated porous media. *Water Resour. Res.* 12, 513–522.
- Raviart, P.A., Thomas, J.M., 1977. A mixed finite element method for second order elliptic problems. In: *Mathematical Aspects of Finite Element Method*, 606. Springer, Berlin, Heidelberg, pp. 292–315. *Lecture Notes in Mathematics*.
- Younes, A., Ackerer, P., Chavent, G., 2004. From mixed finite elements to finite volumes for elliptic PDE in 2 and 3 dimensions. *Int. J. Numer. Methods Eng.* 59, 365–388.
- Moortgat, J., Firoozabadi, A., 2016. Mixed-hybrid and vertex-discontinuous-Galerkin finite element modeling of multiphase compositional flow on 3D unstructured grids. *J. Comput. Phys.* 315, 476–500.
- Vohralík, M., 2006. Equivalence between lowest-order mixed finite element and multi-point finite volume methods on simplicial meshes. *Math. Model. Numer. Anal.* 40 (2), 367–391.
- Farthing, M.W., Kees, C.E., Miller, C.T., 2002. Mixed finite element methods and higher-order temporal approximations. *Adv. Water Resour.* 25, 85–101.
- Tocci, M.D., Kelly, C.T., Miller, C.T., 1997. Accurate and economical solution of the pressure-head form of Richards' equation by the method of lines. *Adv. Water Resour.* 20, 1–14.
- Kavetski, D., Binning, P., Sloan, S.W., 2001. Adaptive backward Euler time stepping with truncation error control for numerical modelling of unsaturated fluid flow. *Int. J. Numer. Methods Eng.* 53, 1301–1322.
- Kees, C.E., Miller, C.T., 2002. Higher order time integration methods for two-phase flow. *Adv. Water Resour.* 25 (2), 159–177.
- Brenan, K.E., Campbell, S.L., Petzold, L.R., 1996. *The Numerical Solution of Initial Value Problems in Differential-Algebraic Equations*. Society for Industrial and Applied Mathematics, Philadelphia, PA.
- Hindmarsh, A.C., Petzold, L.R., 1995. Algorithms and software for ordinary differential equations and differential-algebraic equations. Part II: Higher-order methods and software packages *Comput. Phys.* 9 (2), 148–155.
- Curtis, A.R., Powell, M.J.D., Reid, J.K., 1974. On the estimation of Sparse Jacobian Matrices. *J. Inst. Math. Appl.* 13, 117–119.
- Hindmarsh, A.C., 1982. Large ordinary differential equation systems and software. *IEEE Control Syst. Mag.* 2, 24–30.
- Vauclin, M., Khanji, D., Vachaud, G., 1979. Experimental and numerical study of a transient, two-dimensional unsaturated-saturated water table recharge problem. *Water Resour. Res.* 15, 1089–1101.
- Forsyth, P.A., Kropinski, M.C., 1997. Monotonicity considerations for saturated-unsaturated subsurface flow. *SIAM J. Sci. Comput.* 18, 1328–1354.
- Huang, K., Mohanty, B.P., van Genuchten, M.T., 1996. A new convergence criterion for the modified Picard iteration method to solve the variably saturated flow equation. *J. Hydrol.* 178 (1–4), 69–91.
- United Nations Development Program. Assessment of groundwater resources of Lebanon. Ministry of energy and water, Beirut, Lebanon. 2014.**
- Van Vuuren, D., Edmonds, J., Kainuma, M., Riahi, K., Thomson, A., Hibbard, K., 2011. The representative concentration pathways: an overview. *Clim. Chang.* 109, 5–31.
- FAO, 1970. *Projet De Développement Hydro-Agricole: Etude Hydrogéologique De La Plaine D'Akkar*. République Libanaise. Ministère des Ressources Hydrauliques et Électriques, Beyrouth, Liban.